Strojniški vestnik - Journal of Mechanical Engineering 52(2006)10, 653-661
UDK - UDC 621.165:62-13
Kratki znanstveni prispevek - Short scientific paper (1.03)

Dinamično vedenje vrtilnega sistema turbine

The Dynamic Behavior of a Turbine Rotating System

Vytautas Barzdaitis[1] - Marijonas Bogdevicius[2]
([1]Kaunas University of Technology, Lithuania; [2]Vilnius Gediminas Technical University, Lithuania)

Prispevek s pomočjo teoretičnega modeliranja in simuliranja obravnava dinamiko vrtilnega sistema turbine, skupaj s spremljanjem eksperimentalnih pogojev in diagnosticiranjem rezultatov. Dva rotoja sta povezana z zobniško sklopko s svežnji prožnih plošč. Med ploščami in polvprijemajočimi zobmi so tanke plasti olja. Med ploščami, ploščnimi svežnji in polvprijemajočimi zobmi lahko nastane prožni stik. Dinamični model vrtilnega sistema z zobniškim sklopom smo oblikovali in simulirali. Simulacijske in preizkusne merilne rezultate vrtilnega sistema smo uporabili za razpoznavo vira nihanj ter napak na prožnih ploščah, ki nastanajo zaradi korozijske obrabe in neporavnanosti rotorjev.

(Ključne besede: turbine parne, sistemi rotorski, dinamika, numerične metode, korozija stična)

This paper looks at the dynamics of a steam-turbine rotating system using theoretical modeling and a simulation combined with experimental condition monitoring and diagnostics results. Two rotors are connected by the toothed wheel coupling with elastic plate packets. There are thin layers of oil between the plates and the semi-couplings' teeth. Elastic contacts can occur between the plates, the plate packets and the semi-couplings' teeth. A dynamic model of the rotating system with the toothed-wheel coupling was designed and simulated. The simulation and experimental measurement results of the rotating system were used to identify the vibration sources and the failures of the elastic plates due to fretting corrosion and the misalignment of the rotors.

(Keywords: steam turbines, rotating systems, dynamics, numerical methods, fretting corrosion)

0 INTRODUCTION

The power generating machines in Lithuania are usually steam turbines that have been in service for about 25 to 40 years. The renovation of these machines results in an increase in both reliability and efficiency. The steam-turbine rotor system (Figure 1) consists of two rotors: a high-pressure cylinder rotor (HPR), a medium- and low-pressure cylinder rotor (MLPR), and a toothed-wheel coupling (TWC). The design of the coupling used in high-power turbo generators (60 MW) is modern but not sufficiently applied in practice. Figure 1 b shows a TWC with 80 teeth connected by plate packets. Each plate packet contains three carbon-steel plates: two of them are 7×45×300 mm and one is 2×45×300 mm. The TWC transmits about 70% of the turbine's torque to the MLPR and to the electric generator.

The rotating system with the hydrodynamic journal bearings and the TWC vibrates during the 3000-rpm rotation speed, and this vibration movement is activated by the toothed-wheel coupling with the plate packets. The dynamic movement of each plate in the packet as well as of all the plate packets is complex, but important for the safe continuous operation of the machine, and it is complicated or even impossible to measure the vibration displacement of the plates and the coupling teeth in situ. The TWC plates inside the packet have to operate under unfavorable conditions: high inertia forces, high temperature, variable lubrication and loading, and relative displacements of the semi-couplings with teeth. Furthermore, during dynamic loading a metallic contact between a plate packet and a tooth may occur. The friction between the plates inside a packet and the teeth cause the fretting corrosion phenomenon that damages the plates. Fretting wear will occur in any material under the conditions of cyclic slip under load [1]. Therefore, the operating conditions of plate packets determine their reliability and, in general, the reliability of the whole rotating system. In this paper the machine-condition monitoring and the diagnostic method is evaluated with modeling and simulation of the dynamics of the rotating system with journal bearings and with the TWC plate packets, both theoretically and experimentally.

The dynamic analysis of a non-linear torsion motion flexible coupling with elastic links is presented in [2]. The results of the analysis of the steady running and transient vibration performance are applied to the determination of the optimum proportions of the couplings. Some influence of the flexible coupling's stiffness on the torsion-motion torque amplitude is considered in [3]. The vibration of the high-power asynchronous electric motor of an air blower is estimated by the periodic monitoring of the absolute vibration of the housing bearings and the relative vibrations of the rotor shaft, and is presented [4]. The insufficient *1X* dynamic stiffness of the rotor system is the main reason for the high vibration amplitude of the *1X* frequency in the electric motor. The dynamics of the rotor is investigated using the finite-element method. The complex finite element of the rotor has twenty-six degrees of freedom. The general dynamic model for a large-scale rotor-bearing system with a cracked shaft is presented in reference [5]. The model accommodates shafts with tapered portions, multiple disks and anisotropic bearings. The dynamic processes in the driver together with the asynchronous engine, coupling with gas, and mechanical drive are considered in [6] to [8]. A coupling of this type consists of separate segments, where additional masses are input. The dynamic model of the driver, the pressure-wave propagation in gas, the interaction of separate coupling bodies and gas are studied. The direct mathematical simulation method of the rotor system with an elastic link is presented [9]. The finite-element method approximates a rotor-bearing system with a finite-degree-of-freedom system, the motions of which are described by ordinary differential equations ([10] to [13]).

1 THE DYNAMIC MODEL OF STEAM TURBINE ROTORS

The steam-turbine rotating system is shown in Figure 1 and consists of two rotors supported by oil-film bearings and TWC. The following general assumptions were made: the material of the rotors and the coupling are elastic; shear forces are taken into account; the deflection of the rotor is produced by the displacement of points of the centre line; the axial motion of the rotors is neglected; and the semi-couplings are treated as rigid.

The rotor dynamics is simulated by the finite-element method, where the finite element consists of two nodes and five degrees of freedom (DOF) at each node. The first and the second DOF are displacements along the y and z axes and the last three DOF are angles around the X, Y and Z axes. The vector of translation displacement and the rotation angles of the rotor's finite element can be described as follows:

$$\begin{Bmatrix} v \\ w \end{Bmatrix} = \begin{bmatrix} N_v(\xi) \\ N_w(\xi) \end{bmatrix} \{q(t)\} = [N]\{q\}$$

$$\{\theta\} = \begin{Bmatrix} \alpha \\ \beta \\ \gamma \end{Bmatrix} = \begin{bmatrix} N_{1\theta}(\xi) \\ N_{2\theta}(\xi) \\ N_{3\theta}(\xi) \end{bmatrix} \{q(t)\} = [N_\theta]\{q\} \qquad (1),$$

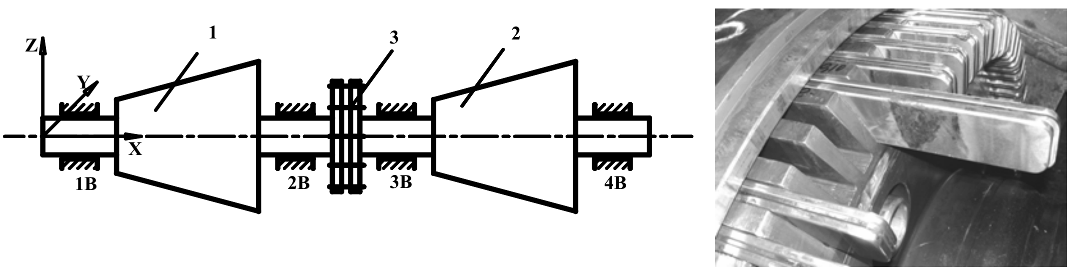

a) b)

Fig. 1. *Rotors and bearings layout: a – rotating system, 1 – HPR, 2 – MLPR, 3 – TWC, 1B and 3B – radial-axial bearings, 2B and 4B radial bearing; b - view of TWC with plate packets*

where $\{q\}$ is the nodal element displacement vector; $[N]$ and $[N_\theta]$ are the matrices of the shape functions (see appendix A).

Cardin's angles are used to determine the relationship between the angular velocity $\{\dot{\theta}\}$ and the angular velocity $\{\omega\}$ in the XYZ coordinate system.

The equations of motion of the rotor's finite element are derived by applying a Lagrange equation of the second order, which can be written as follows:

$$\left[M(q)\right]\{\ddot{q}\}+\left([C]+[G]\right)\{\dot{q}\}+[K]\{q\}=\left\{F(q,\dot{q})\right\} \quad (2),$$

where $[M(q)]$, $[C]$, $[G]$ and $[K]$ are the mass, damping, gyroscopic and stiffness matrices of the finite element, respectively (see appendix B); and $\left\{F(q,\dot{q})\right\}$ is the load vector of the finite element.

2 BEARING MODEL

Under the assumption of small displacements of the journal centre, the fluid-film force components in the horizontal and vertical directions, F_y and F_z, turn out to be as follows:

$$\{F_b\}=\begin{bmatrix} c_{yy} & c_{yz} \\ c_{zy} & czz \end{bmatrix}\begin{Bmatrix} \dot{v} \\ \dot{w} \end{Bmatrix}+\begin{bmatrix} k_{yy} & k_{yz} \\ k_{zy} & k_{zz} \end{bmatrix}\begin{Bmatrix} v \\ w \end{Bmatrix}=[C_b]\begin{Bmatrix} \dot{v} \\ \dot{w} \end{Bmatrix}+[K_b]\begin{Bmatrix} v \\ w \end{Bmatrix} \quad (3),$$

where k_{ij} and c_{ij} $(i,j) = (Y,Z)$ are the stiffness and damping coefficients, respectively (Figure 2).

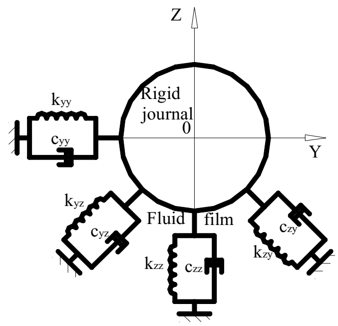

Fig. 2. *Fluid-film bearing model*

3 COUPLING MODEL

The rotors and the bearing system are considered in the global coordinate system XYZ (Figure 1). The semi-couplings are considered as a rigid body attached to the rotors. The mass centers of the first and second semi-couplings are input into the moving coordinate systems $X_1Y_1Z_1$, $X_2Y_2Z_2$, respectively. Each semi-coupling contains notches where a package of three plates is inserted. In each notch of the first and second semi-coupling coordinate systems $X_{1k}Y_{1k}Z_{1k}$ and $X_{2k}Y_{2k}Z_{2k}$ are input, respectively, where $k = 1,2,...,NZ$ and NZ is the number of notches (Figure 3).

The coordinates vector of point P_i in the global coordinate system XYZ in the i^{th} semi-coupling and in the k^{th} notch are given by:

$$\{R_{pi}\}=\{R_{ci0}\}+\{U_{ci}\}+[A_i]\left(\{r_{ik,0}\}+\left[A_3(\gamma_k)\right]\{r_{ik,1}\}\right) \quad (4),$$

where:

- $\{R_{ci0}\}$ is the initial coordinate vector of the mass centre point C_i of the i^{th} semi-coupling;
- $\{U_{ci}\}$ is the vector translation displacements of the point C_i;
- $[A_i]$ is the transformation matrix between the coordinate systems XYZ and $X_iY_iZ_i$;
- γ_k is the angle $\gamma_k = 3\pi/2 + \alpha_k$, $\alpha_k = (k-1)2\pi/NZ$, $(k=1,2,...,NZ)$;

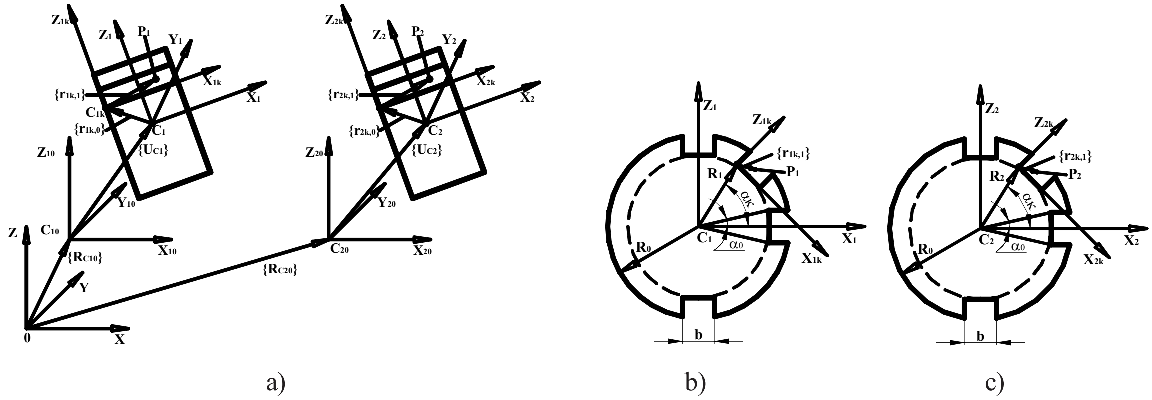

Fig. 3. *The TWC model: a – coupling; b – HPR semi-coupling; c – MLPR semi-coupling*

- $[A_3(\gamma_k)]$ is the transformation matrix between the coordinate system $X_1Y_1Z_1$ and $X_{1k}Y_{1k}Z_{1k}$,
- $\{r_{ik,0}\}$ is the vector that is equal to $\{r_{ik,0}\} = [-\alpha_1 \quad R_1\cos(\alpha_k+\alpha_0) \quad R_1\sin(\alpha_k+\alpha_0)]$; $\sin(\alpha_0) = b/2R_1$; and
- $\{r_{ik,1}\}$ is the vector that determines the coordinates of the point P_i in the coordinate system $X_{ik}Y_{ik}Z_{ik}$, $(i=1,2)$.

The vector $\{d_{12k}\}$ from point P_1 to P_2 in the k^{th} notch and in the $X_{1k}Y_{1k}Z_{1k}$ coordinate system is equal to:

$$\{d_{12k}\} = [A_3]^T[A_1]^T\left(\{R_{p2}\}-\{R_{p1}\}\right) \tag{5}$$

and its first time-derivative is developed:

$$\{\dot{d}_{12k}\} = [A_3]^T\left[\dot{A}_1\right]^T\left(\{R_{p2}\}-\{R_{p1}\}\right)+[A_3]^T[A_1]^T\left(\{\dot{R}_{p2}\}-\{\dot{R}_{p1}\}\right) \tag{6}$$

where $\left[\dot{A}_i\right]=[\tilde{\omega}_i][A_i]$;
$\{\dot{R}_{pi}\}=\{\dot{U}_{ci}\}+\left[\dot{A}_i\right]\left(\{r_{ik,0}\}+[A_3(\gamma_k)]\{r_{ik,1}\}\right)$;
$[\tilde{\omega}_i]$ is a skew-symmetric matrix associated with the vectors $\{\omega_i\}=\left[\Omega+\dot{\alpha}_i \quad \dot{\beta}_i \quad \dot{\gamma}_i\right]$, $(i=1,2)$, respectively.

The elements of the vector of force acting in the kth notch of the first and the second semi-coupling in the $X_{1k}Y_{1k}Z_{1k}$ coordinate system are given as:

$$F_{2ky}=\begin{cases} -k_y\left(d_{12k}(2)-\delta_y\right), & if \ d_{12k}(2)>\delta_y \\ -c_{y,fluid}\dot{d}_{12k}(2), & if \ -\delta_y\le d_{12k}(2)\le\delta_y \\ -k_y\left(d_{12k}(2)+\delta_y\right), & if \ d_{12k}(2)<-\delta_y \end{cases}$$

$$\begin{gathered} F_{2kx}=-f\left|F_{1ky}\right|sign\left(\dot{d}_{12k}(1)\right) \\ F_{2kz}=-f\left|F_{2ky}\right|sign\left(\dot{d}_{12k}(3)\right) \\ \{F_{2k}\}=\left[F_{2kx} \quad F_{2ky} \quad F_{2kz}\right]^T \\ \{F_{1k}\}=-\{F_{2k}\} \end{gathered} \tag{7}$$

where δ_y is the gap between the k^{th} plate and the semi-coupling; k_y, k_z and $c_{y,\text{fluid}}$ are coefficients of stiffness and damping of the k^{th} plate; f is the friction coefficient between the plate and the semi-coupling.

The following total force and moment vectors acting at points C_i in the global coordinate system are developed as follows:

$$\begin{gathered} \{F_{ci}\}=[A_i]\sum_{k=1}^{NZ}[A_3(\gamma_k)]\{F_{ik}\} \\ \{M_{ci}\}=[A_i]\sum_{k=1}^{NZ}\left[\tilde{r}_{k,ci,pi}\right][A_3(\gamma_k)]\{F_{ik}\} \end{gathered} \tag{8}$$

where $\left[\tilde{r}_{k,ci,pi}\right]$ is a skew-symmetric matrix associated with vectors:

$$\{r_{k,ci,pi}\}=\{r_{ik,0}\}+[A_3(\gamma_k)]\{r_{ik,1}\}$$
$$(i=1,2)$$

The equations of motion of the coupling can be presented by the matrix equation:

$$\left[M_{coupl}\left(q_{coupl}\right)\right]\{\ddot{q}_{coupl}\}+\left[G_{coupl}\right]\{\dot{q}_{coupl}\}=\left\{F_{coupl}\left(q_{coupl},\dot{q}_{coupl}\right)\right\} \tag{9}$$

where $[M_{\text{coupl}}(q_{\text{coupl}})]$, $[G_{\text{coupl}}]$ and $[K_{\text{coupl}}]$ are mass and gyroscopic matrices of the coupling, respectively (see appendix C); and $\left\{F_{coupl}\left(q_{coupl},\dot{q}_{coupl}\right)\right\}$ is the load vector of the coupling.

4 THE SOLUTION OF THE DYNAMIC EQUILIBRIUM EQUATION

The dynamic equilibrium equation for the structure is written as follows:

$$[M(q)]\{\ddot{q}\}+[C]\{\dot{q}\}+[K]\{q\}=\{P(t)\}+\{F(t,q,\dot{q})\} \tag{10}$$

where $[M(q)]$, $[C]$ and $[K]$ are the mass, damping and stiffness matrices; $\{P(t)\}$ is an externally applied load vector; $\{F(t,q,\dot{q})\}$ is a non-linear force vector; and $\{q\},\{\dot{q}\}$ and $\{\ddot{q}\}$ are the displacement, velocity and acceleration vectors of the finite-element assemblage. In an implicit time-integration scheme, the equilibrium of the system (10) is considered at time $t+\Delta t$ to obtain the solution at time $t+\Delta t$. Iteration will be performed in the non-linear analysis. Using the Newton-Raphson iteration method, the main equilibrium equations turned out to be as follows:

$$\begin{gathered} [M]_{t+\Delta t,i-1}\{\ddot{q}\}_{t+\Delta t,i}+[C]_{t+\Delta t,i-1}\{\dot{q}\}_{t+\Delta t,i} \\ +\left([K]_{t+\Delta t,i-1}-[J]_{t+\Delta t,i-1}\right)\{\Delta q\}_i= \\ \{P\}_{t+\Delta t}+\{F\}_{t+\Delta t,i-1} \end{gathered} \tag{11}$$

$$\{q\}_{t+\Delta t,i}=\{q\}_{t+\Delta t,i-1}+\{\Delta q\}_i$$

where $[J]_{t+\Delta t,i-1}$ is Jacobian matrix, $[J]_{t+\Delta t,i-1}=[\partial\{F\}/\partial\{q\}_T]$.

In the Newmark-Beta time-integration scheme, the following assumptions are employed ([4] and [14]):

$$\begin{gathered} \{q\}_{t+\Delta t}=\{q\}_t+\frac{\Delta t}{2}\left(\{\dot{q}\}_t+\{\dot{q}\}_{t+\Delta t}\right) \\ \{\dot{q}\}_{t+\Delta t}=\{\dot{q}\}_t+\frac{\Delta t}{2}\left(\{\ddot{q}\}_t+\{\ddot{q}\}_{t+\Delta t}\right) \end{gathered} \tag{12}$$

The application of the relations of the equations (12) results in:

$$\{\ddot{q}\}_{t+\Delta t,i}=\frac{4}{\Delta t^2}\left(\{q\}_{t+\Delta t,i-1}-\{q\}_t+\{\Delta q\}_i\right)-\frac{4}{\Delta t}\{\dot{q}\}_t-\{\ddot{q}\}_t \tag{13}$$

and substituting into Equation (11) yields:

$$\left(\frac{4}{\Delta t^2}[M]_{t+\Delta t,i-1}+\frac{2}{\Delta t}[C]+[K]-[J]_{t+\Delta t,i-1}\right)\{\Delta q\}_i=\{P\}_{t+\Delta t}+$$
$$\{F\}_{t+\Delta t,i-1}-[M]\left(\frac{4}{\Delta t^2}\left(\{q\}_{t+\Delta t,i-1}-\{q\}_t\right)-\frac{4}{\Delta t}\{\dot{q}\}_t-\{\ddot{q}\}_t\right)-$$
$$[C]\left(\frac{2}{\Delta t}\left(\{q\}_{t+\Delta t,i-1}-\{q\}_t\right)-\{\dot{q}\}_t\right) \qquad (14).$$

The selection of an appropriate time step Δt is important for the accuracy of the simulation results. A time step of 10^{-5} s was selected to be used in the integration process.

5 RESULTS AND DISCUSSION

The values of the stiffness coefficients of the bearings are as follows: k_{yy} = 100.0×10^6 N/m, k_{yz} = 50.0×10^6 N/m, k_{zy} = –20.0×10^6 N/m, k_{zz} = 300.0×10^6 N/m, c_{yy} = c_{zz} = 50.0×10^3 Ns/m, and c_{yy} = c_{zz} = 0. The steel's density and the elastic modulus are ρ = 7850 kg/m^3 and E = 210×10^9 N/m^2, respectively. The gap between the plate packet and the semi-coupling is equal to δ = 90×10^{-6} m. The coefficients of stiffness and the damping of the plate packet are k_y = 7.47×10^9 N/m, k_z = 1.050×10^9 N/m, c_y = 5.0×10^3 Ns/m, respectively, and the friction coefficient between the plate and the semi-coupling teeth is equal to f = 0.10. The radii of the coupling are R_0 = 0.424 m, and R_1 = R_2 = 0.374 m. The geometrical parameters of the coupling are a_1 = a_2 = 0.035 m, and b = 15.180×10^{-3} m. The mass, polar and transverse moments of the semi-coupling are m_1 = m_2 = 241 kg, J_{cp} = 2.15×10^{-3} m^4, and J_{cd} = 1.075×10^{-3} m^4. The journal diameter is equal to 0.300 m with the length 0.300 m; the bearing radial clearance "lemon type" is ~350×10^{-6} m. The turbines transferred to a 40 MW power load. The unbalances of the rotors are negligible.

The vibration caused by the TWC falls in the high-frequency region from 3000 Hz up to 7000 Hz, as shown in Fig. 4. Experimental results indicated that a more accurate parameter to evaluate the technical condition of the TWC is the 2nd bearing's absolute vibration acceleration in comparison with the 1st and 3rd bearings' vibration data [15]. The prevailing vibration acceleration amplitudes at ~4000 Hz frequency indicate that such a high-frequency vibration is caused by TWC plate packets meshing with teeth as in gear drivers (80 packets × 50 Hz = 4000 Hz).

The vibration acceleration spectra acquired from the experimental monitoring of the 2nd bearing indicates a significant difference in the vibration amplitudes at frequencies of 3180 to 4100 Hz when the TWC runs with new plates (a), in comparison with the vibration intensity of the TWC with used damaged plates (b), as shown in Fig. 4. The TWC with damaged plates provides not only high-frequency (~4000 Hz) acceleration amplitudes but 6000 to 6500 Hz vibration accelerations. These data approved the diagnostics concept of the TWC condition evaluation with high-frequency acceleration monitoring of the 2nd bearing. The surfaces of the plates that are in contact with the MLPR were heavily damaged in comparison with the driven sides of the plates that are in contact with the HPR.

If the load is increased up to 53 MW, the vibration intensity of these frequencies slightly decreases. It can be interpreted as a more uniform transmission motion of the rotating system torque from the driving part of the coupling via the plate packets and teeth to the driven part of the coupling, since larger deformations of the plates in the TWC distribute the load among the plate packets more uniformly.

The experimental study of the kinetic orbits of the 2nd and 3rd bearing shafts indicates that the maximum value of the 2nd shaft displacement from the time-integrated mean position "zero"

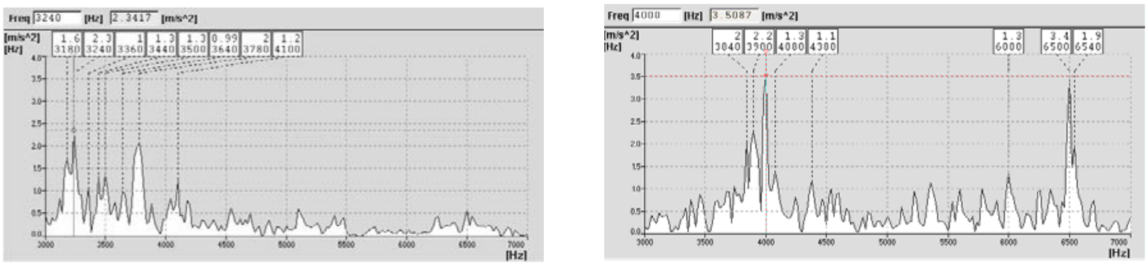

a - new plates

b - used and damaged plates

Fig.4. *2nd bearing's vertical vibration accelerations spectra with TWC new plates (a) and with plates used in the exploitation and finally damaged (b)*

s_{max2}=158 µm is three times larger in comparison with the 3rd shaft s_{max3}=55 µm, as shown in Fig.5. It is impossible to measure the semi-couplings' orbits, but the HPR semi-coupling orbit repeats the 2nd shaft's motion as the MLPR semi-coupling orbit, i.e., the 3rd shaft.

The data of the average position changes of the HPR and MLPR bearing's shafts is presented in Table 1. The changes in the HPR 3rd bearing shaft's average position in the bearing during 10 months in operation indicates the significant changes in the static radial loads acting on the MLPR. The 3rd bearing shaft position's changes in the fluid-film bearing versus time indicate a misalignment malfunction of the HPR-MLPR. The heavy damage to the plate's surfaces took place in the contact area with MLPR semi-coupling teeth (Fig. 1b), but not with HPR semi-coupling teeth. The HPR with the semi-coupling and the plate packets moves in a radial direction relative to the LMPR semi-coupling teeth. This motion provides additional friction between the plates and the LMPR teeth.

The theoretical simulation results of the rotating system model confirmed that the causality of the plate's damage was only slightly involved in the vibration displacement of the plates in the packets that caused the fretting corrosion of the plates. The simulated vibration displacements under a 40 MW power load during four full rotations indicated that the HPR and MLPR semi-couplings' vibration displacements in the *XYZ* coordinate system reached 140 µm in the *Y* (Fig.6) and *Z* directions.

Simulated vibration displacements of the first plate packet during a full four rotations in the $X_{1k}Y_{1k}Z_{1k}$ coordinate system at a 40 MW power load is shown in Fig. 7, and comprises maximum peak-peak values of s_{ppmax}=150 µm. The contact between the plates and the plate packet with the semi-coupling tooth is not constant, and the oil pressure in this gap is variable. Such an operating condition of the plate packet is caused by the relative motion of the mated contact surfaces and results in contact failures and fretting corrosion and increased damage to the plates. Due to continuous long-term operation, heavy damage to the plates is caused by the eccentric motion of HPR-MLPR due to the misalignment.

6 CONCLUSIONS

1. The designed theoretical model of the whole rotating system is based on the finite-element method and simulates the dynamics parameters of elements, and the vibration displacements of

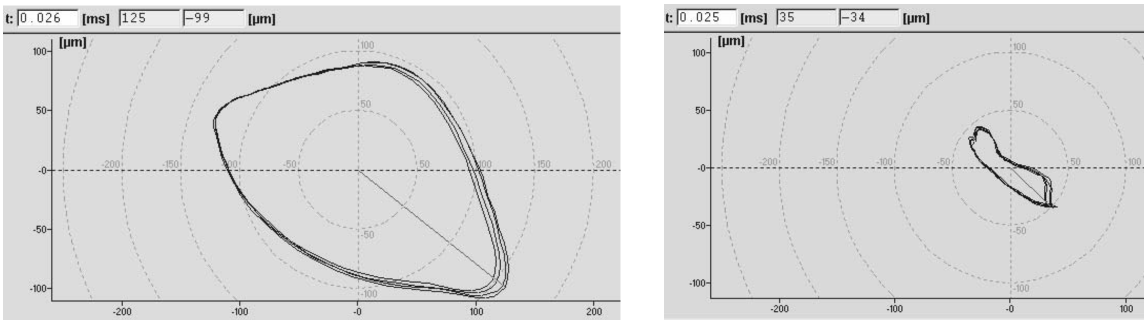

2nd bearing's shaft, s_{max2}=158 µm 3rd bearing's shaft, s_{max3}=55 µm

Fig. 5. *The kinetic orbits of 2nd and 3rd bearings' shafts measured with proximity probes*

Table 1. *The average shaft positions in the bearings during 10 months of steady-state operation*

Machine Operation conditions	HPR bearings shafts' gaps, in µm				MLPR bearings shafts' gaps, in µm			
	1st bearing		2nd bearing		3rd bearing		4th bearing	
	XY displacement directions, when rotating system runs in CW direction							
	-1X	+1Y	-2X	+2Y	-3X	+3Y	-4X	+4Y
After overhaul	-135	+268	-151	+375	-276	+271	-130	+407
After 10 months	-195	+365	-167	+399	-349	+203	-143	+423

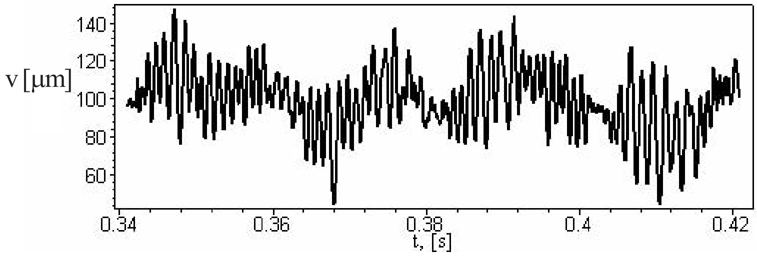

Fig. 6. *Vibration displacement $s_y(t)$ plot of the HPR semi-coupling during a full four rotations in the XYZ coordinate system under a 40 MW power load in the horizontal Y direction*

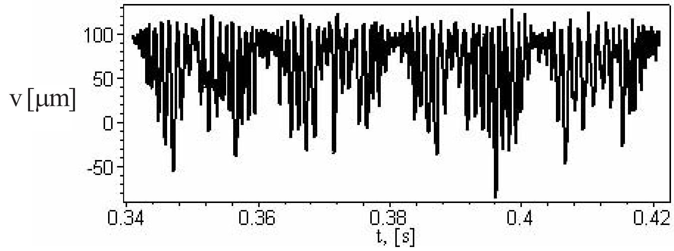

Fig. 7. *Vibration displacement plot of the first plate packet in the $X_{1k}Y_{1k}Z_{1k}$ coordinate system in the Y_{1k} direction*

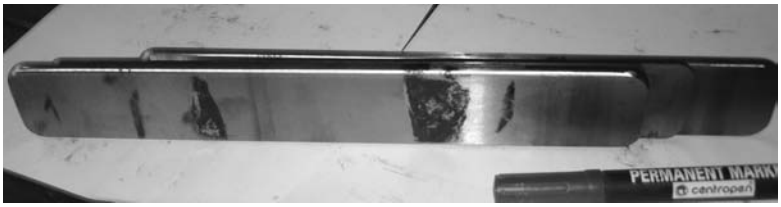

Fig. 8. *Photograph of the damaged plate of the TWC caused by the fretting corrosion and misalignment of the HPR - LMPR*

the tooth-wheel coupling elements that are impossible to measure in-situ on the running machine. The gyroscopic effect due to the rotor's spinning motion and the dynamic properties of the oil-film bearings were introduced in the model.

2. Theoretical and experimental research results identify the causality that provides heavy damage to the TWC plates: the vibration displacements of the rotors, plates and plate packets, and the misalignment of the HPR due to the MLPR.
3. The results indicated that an accurate parameter to evaluate the technical condition of the toothed-wheel coupling is the HPR 2nd bearing's absolute high-frequency vibration acceleration.

APPENDIX A

Individual shape functions given by Ref. [10] are:

$$N_1 = \frac{1}{1+\Phi}\left(1 - 3\xi^2 + 2\xi^3 + \frac{\Phi}{2}(1-\xi)\right)$$

$$N_2 = \frac{L}{1+\Phi}\left(\xi - 2\xi^2 + \xi^3 + \frac{\Phi}{2}\xi(1-\xi)\right)$$

$$N_3 = \frac{1}{1+\Phi}\left(3\xi^2 - 2\xi^3 + \Phi\xi\right)$$

$$N_4 = \frac{L}{1+\Phi}\left(-\xi^2 + \xi^3 + \frac{\Phi}{2}\xi(\xi-1)\right)$$

$$N_5 = 1-\xi; \quad N_6 = \xi$$

$$N_7 = \frac{-6\xi}{L(1+\Phi)}(1-\xi); \qquad N_8 = \frac{1}{1+\Phi}\left(1 - 4\xi + 3\xi^2 + \Phi(1-\xi)\right)$$

$$N_9 = \frac{6\xi}{L(1+\Phi)}(1-\xi); \qquad N_{10} = \frac{1}{1+\Phi}\left(-2\xi + 3\xi^2 + \Phi\xi\right)$$

$$[N] = \begin{bmatrix} N_1 & 0 & 0 & 0 & N_2 & N_3 & 0 & 0 & 0 & N_4 \\ 0 & N_1 & 0 & -N_2 & 0 & 0 & N_3 & 0 & -N_4 & 0 \end{bmatrix}$$

$$[N_\theta] = \begin{bmatrix} 0 & 0 & \frac{dN_5}{d\xi} & 0 & 0 & 0 & 0 & \frac{dN_6}{d\xi} & 0 & 0 \\ 0 & -\frac{dN_7}{d\xi} & 0 & \frac{dN_8}{d\xi} & 0 & 0 & -\frac{dN_9}{d\xi} & 0 & \frac{dN_{10}}{d\xi} & 0 \\ \frac{dN_7}{d\xi} & 0 & 0 & 0 & \frac{dN_8}{d\xi} & \frac{dN_9}{d\xi} & 0 & 0 & 0 & \frac{dN_{10}}{d\xi} \end{bmatrix}$$

Φ - the shear deformation parameter, $\Phi = 12EJ_d/kGAL^2$;
E, G - moduli of elasticity and shear respectively;
A - cross-sectional area;
J_d is the second moment of the cross-sectional area;
k - the shear correction factor depending on the shape of the cross-section;
ξ - the non-dimensional natural coordinate, $\xi = x/L$.

APPENDIX B

The stiffness matrix of the rotor's finite element is:

$$[K] = [K_{11}] + [K_{12}] + [K_{21}] + [K_{22}] + [K_3]$$

$$[K_{11}] = \int_0^L \left[\frac{dN_{1\beta}}{dx}\right]^T EJ_d \left[\frac{dN_{1\beta}}{dx}\right] dx$$

$$[K_{12}] = \int_0^L \left[\frac{dN_{2\beta}}{dx}\right]^T EJ_d \left[\frac{dN_{2\beta}}{dx}\right] dx$$

$$[K_{21}] = \int_0^L \left(\left[\frac{dN_v}{dx}\right] - [N_{2\beta}]\right)^T kGA \left(\left[\frac{dN_v}{dx}\right] - [N_{2\beta}]\right) dx$$

$$[K_{22}] = \int_0^L \left(\left[\frac{dN_w}{dx}\right] + [N_{2\beta}]\right)^T kGA \left(\left[\frac{dN_w}{dx}\right] + [N_{2\beta}]\right) dx$$

$$[K_3] = \int_0^L [N_{1\theta}]^T GJ_p [N_{1\theta}] dx$$

The total kinetic energy of the rotor's finite element in short form is:

$$T = \frac{1}{2}\rho L J_p \Omega^2 + \frac{1}{2}\{\dot{q}\}^T [M]\{\dot{q}\} + \Omega [P_1]\{\dot{q}\} - \Omega \{q\}^T [P_2]\{\dot{q}\}$$

where $[M]$ is the composite mass matrix of the rotor's finite element is:

$$[M] = [M_1] + [M_2] - [M_3(q$$

$$[P_1] = \int_0^1 \rho L J_p [N_{1\theta}] d\xi$$

$$[P_2] = \int_0^1 \rho L J_p [N_{2\theta}]^T [N_{3\theta}] d\xi$$

$$[M_1] = \int_0^1 \rho L [N]^T [N] d\xi$$

$$[M_2] = 2L \int_0^1 [N_\theta]^T [D_1][N_\theta] d\xi$$

$$[M_3(q)] = \int_0^1 [N_{1\theta}]^T \left(L\rho J_p \theta_y\right)[N_{3\theta}] d\xi$$

$$[D_1] = diag\left[\rho J_p \quad \rho J_d \quad \rho J_d\right]$$

where A is cross-sectional area; ρ is density of the finite element; J_p, J_d are the polar and transverse moments, respectively; Ω is the constant angular velocity of rotor.

The gyroscopic matrix of the rotor's finite element is:

$$[G] = \Omega\left([P_2] - [P_2]^T\right)$$

APPENDIX C

The mass and gyroscopic matrices of the semi-coupling can be:

$$[M_c] = L_c([D_3] + 2\beta[D_6])$$

$$[G_c] = L_c \Omega\left([D_4] - [D_4]^T\right)$$

$$[D_3] = \begin{bmatrix} \begin{bmatrix} \rho A_c & 0 \\ 0 & \rho A_c \end{bmatrix} & [0] \\ [0] & [D_1] \end{bmatrix}$$

$$[D_4] = \rho J_{cp} \begin{bmatrix} 0 & 0 & 0 & 0 & 0 \\ 0 & 0 & 0 & 0 & 0 \\ 0 & 0 & 0 & 0 & 0 \\ 0 & 0 & 0 & 0 & 0 \\ 0 & 0 & 0 & -1 & 0 \end{bmatrix}$$

$$[D_2] = [D_0]^T [D_1][D_0]$$

$$[D_0] = \begin{bmatrix} 1 & 0 & -\beta \\ 0 & 1 & \alpha \\ 0 & -\alpha & 1 \end{bmatrix}$$

$$[D_1] = \begin{bmatrix} \rho J_{cp} & 0 & 0 \\ 0 & \rho J_{cd} & 0 \\ 0 & 0 & \rho J_{cd} \end{bmatrix}$$

$$[D_6] = \rho J_{cp} \begin{bmatrix} 0 & 0 & 0 & 0 & 0 \\ 0 & 0 & 0 & 0 & 0 \\ 0 & 0 & 0 & 0 & -1 \\ 0 & 0 & 0 & 0 & 0 \\ 0 & 0 & 0 & 0 & 0 \end{bmatrix}$$

where A_c, J_{cp} are the cross-sectional area, polar and transverse inertia moments of the semi-coupling, respectively.

7 REFERENCES

[1] Van Dijk P., Van Meijl (1995) Solutions for contact problems due to fretting corrosion. *VDE- Fachbericht* 47, 13. KontaktSeminar 4-6.

[2] Bert C.W., Wu S.(2003) Dynamic analysis of a nonlinear torsion flexible coupling with elastic links. *Journal of Mechanical Design.* Vol.125, Issue 3, 509-517.

[3] Domachowski Z., Prochnicki W., Puhaczewski Z., Dzida M. (2003) Influence of control loop on torsional vibrations of rotating machinery. *The 2nd International Symposium on Stability Control of Rotating Machinery*. Gdansk-Poland, 4-8 August, 122-129.
[4] Barzdaitis V., Bogdevicius M., Gečys S. (2003) Vibration problems of high power air blower machine. *The 2nd International Symposium on Stability Control of Rotating Machinery (ISCORMA-2)*, Gdansk, 4 -8 August, 606 – 616.
[5] Mohiuddin M.A., Khulief Y.A. (2002) Dynamic response analysis of rotor-bearing systems with cracked shaft. *Journal of Mechanical Design*. Vol.124, Issue 4, 690-696.
[6] Bogdevicius M. (2002) Simulation of dynamic processes in mechanical drive with coupling gas. *Proceedings of the Six International Conference on Motion and Vibration Control*, August 19-23, Saitama, Japan, 543-546.
[7] Bogdevicius M. (2000) Simulation of dynamic processes in hydraulic, pneumatic and mechanical drivers and their elements. Vilnius: *Technika*, 96 p.
[8] Aladjev V., Bogdevičius M. (2001) Maple 6: Solution of the mathematical, statistical and engineering – physical problems. Moscow: *Laboratory of Basic Knowledges*. 824 p. (in Russian).
[9] Bogdevičius M., Spruogis B. (1997) Dynamic and mathematical models of rotor system with elastic link in the presence of shafts misalignment. 2nd *International Conference of Mechanical Engineering "Mechanics'97"*. Proceedings. Part 1. Vilnius: Technika, 78-84.
[10] Nelson H.D. (1980) A finite rotating shaft element using Timoshenko beam theory. *Journal of Mechanical Design*. 102, 793-803.
[11] Rouch K.E., Kao JS. (1979) A tapered beam finite element for rotor dynamics analysis. *Journal Sound and Vibration*, 66, 119-140.
[12] Gmur TC., Rodrigues JD. (1991) Shaft finite element for rotor dynamics analysis. *Journal of Vibration and Acoustics*, 113, 482-493.
[13] Yih-Hwang Lin, Sheng-Cheng Lin (2001) Optimal weight of rotor systems with oil-film bearings subjected to frequency constraints. *Finite Elements in Analysis and Design*, 37 , 777-798.
[14] M.Kawakami, H.Shiojiri (1985) Thermal-elasti-plastic analysis with a plate/shell element using ADINAT/ ADINA. *Computers & Structures*, Vol. 21, No 1/2, 65-177.
[15] Barzdaitis V., Barzdaitis V.V., Did□iokas R., Pocius Z. (2003) Inconsistence of absolute and relative vibration in rotors diagnostics.- Mechanika. ISSN 1392-1207.-Kaunas: *Technologija* , Nr.3(41), 48-54.
[16] Aladjev V., Bogdevičius M., Prentkovskis O. (2002) New software for mathematical package Maple of releases 6,7 and 8. Monograph. Vilnius: *Technika*, 404 p.

Authors' Address: Prof. Dr. Vytautas Barzdaitis
Kaunas University of Technology
Faculty of Mechanical and Mechatronics
K. Donelaičio St. 73
LT-44029 Kaunas, Lithuania
vytautas.barzdaitis@ktu.lt

Prof. Dr. Marijonas Bogdevicius
Vilnius Gediminas Technical Univ.
Faculty of Transport Engineering
Plytines St. 27
LT-10105 Vilnius, Lithuania
marius@ti.vtu.lt

Prejeto: Received: 10.1.2005
Sprejeto: Accepted: 23.2.2006
Odprto za diskusijo: 1 leto
Open for discussion: 1 year